

Concrete filled double skin tubular members subjected to bending

Kojiro Uenaka[†]

*Dept. of Civil Engineering, Kobe City College of Technology Gakuenhigashimachi 8-3,
Nishi, Kobe, 651-2194, Japan*

Hiroaki Kitoh

Dept. of Urban Engineering, Osaka City University, Japan

Keiichiro Sonoda

Professor Emeritus Osaka City University, Japan

(Received June 7, 2007. Accepted April 16, 2008)

Abstract. A concrete filled double skin tubular (called CFDST in abbreviation) member consists of two concentric circular steel tubes and filled concrete between them. Purpose of this study is to investigate their bending characteristics experimentally. The two test parameters of the tubes considered were an inner-to-outer diameter ratio and a thickness-diameter ratio. As a result, their observed failure modes were controlled by tensile cracking or local buckling of the outer tube. Discussion is focused on the confinement effect on the filled concrete due to the both tubes and also the influence of the inner-to-outer diameter ratios on their deformability and load carrying capacity.

Keywords : composite columns; concrete filled double tubular steel member; bending moment capacity; confined effect.

1. Introduction

Concrete filled double steel tubular, called CFDST hereafter in abbreviation, sections are shown in Fig. 1(a), (b) and (c), those consists of two concentric circular steel tubes and filled concrete between them. Comparing CFDST section with an ordinary concrete filled steel tubular, so called CFT, section (Architectural Institute of Japan 1997 and 2002), as also shown in Fig. 1(d), a self weight reduction due to its central hollow space can be anticipated. When CFDST member is applied to a high raised bridge pier, therefore, the reduction can draw the smaller scaled substructures' dimension beneath the pier because of a decreased seismic force to be induced by the light weighted CFSDT pier

Reviewing the past studies on CFDST, we can first find the experimental and analytical studies (Wei *et al.* 1995a, 1995b) on double steel tubes and filled polymer concrete for marine structural application.

[†]Associate Professor, Corresponding author, E-mail: uenaka@kobe-kosen.ac.jp

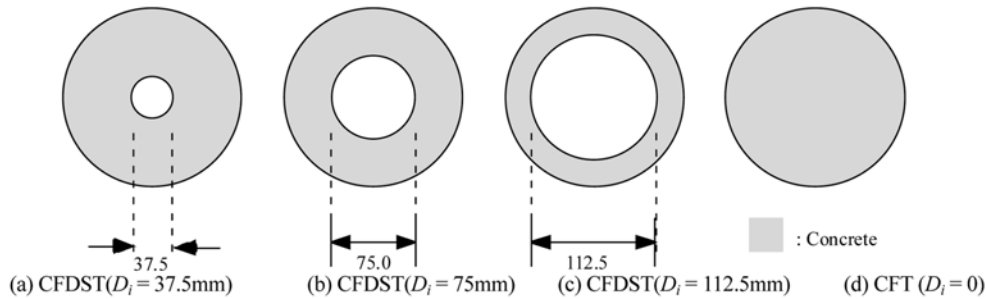


Fig. 1 Cross section of specimens

In the followings, axially compressive tests were conducted on CFDST with four different combinations of outer (square or circular) and inner (square or circular) tubes (Zhao and Grzebieta 2002, Zhao *et al.* 2002a, 2002b, Elchalakani *et al.* 2002), and a study on constitutive law of filled concrete (Tawaratani *et al.* 1999) are also found. On the other hand, for application to earthquake resistance structures, horizontal cyclic loading tests of long CFDST column under a constant axial load were carried out (Yagishita *et al.* 2000), which had reported that a CFDST column had a good deformability and large toughness. Approximate calculation of bending strength of double square skin tube were carried out Zhao and Grzebieta (2002c). A detailed review on CFDST can also be found in Zhao and Han (2006).

Under the background mentioned above, the authors had previously made a parametric study on axially compressive characteristics of CFDST members (Uenaka *et al.* 2003), in which parameters were taken as thickness-to-outer diameter ratio (D_o/t_o), and inner-to-outer diameter ratio (D_i/D_o). From the results obtained by those studies, we could find that (1) a larger D_i/D_o led smaller confined effect of filled concrete and consequently lower ultimate strengths were resulted in. The parameters D_o/t_o and D_i/t_i in this testing program are outside the range being reported in the literature.

This study is, therefore, devoted to investigate bending characteristics of CFDST members through a pure bending test of twelve specimens with various combinations of D_o/t_o and D_i/D_o . Special attentions are placed herein on the confined effect of filled concrete in bending-compression and bending-tension regions, and the associated loading capacities.

2. Experiments

2.1 Test specimens and testing apparatus

The details of all the specimens used herein are listed in Table 1, and their cross sectional views are also shown in Fig. 1. All of them commonly had 450 mm in height: H and 160 mm in outer tube diameter: D_o . Whereas, the both tube thicknesses: t_o and t_i were varied as 1.0, 1.6 or 2.3 mm. Furthermore, the outer tube's diameter-to-thickness ratios were also varied as 69.6, 100 or 200. The self weight reduction ratio of CFDST's to CFT's: $W_{\text{CFDT}}/W_{\text{CFT}}$ were, consequently, ranging from 0.57 to 0.99 as also listed in Table 1. In addition, Young's Modulus: E_s and yielding point: f_y of the tubes obtained by each coupon test also are therein.

We regarded biaxial gauges attachment on both the tubes as important, by only those gauges confinement stress in the filled concrete could be measured at the assemblage of steel element. After molding a flat steel plate into a round shape, the outer tube was welded to end joint plates to be

Table 1 List of Specimens

No.	Tag	Steel Tube						Concrete				$\frac{W_{CFDST}}{W_{CFT}}$
		D_o (mm)	D_i (mm)	D_i/D_o	t_o, t_i (mm)	D_o/t_o	D_i/t_i	E_s (GPa)	f_y (MPa)	E_c (GPa)	f_c (MPa)	
1	m10-000	160.0	0.0	0.00	1.0	160.0	-	250	286	24.2	25.7	1.00
2	m10-375	160.0	37.5	0.23	1.0	160.0	37.5	250	286	24.2	25.7	0.97
3	m10-750	160.0	75.0	0.47	1.0	160.0	75.0	250	286	24.2	25.7	0.83
4	m10-1125	160.0	112.5	0.70	1.0	160.0	112.5	250	286	24.2	25.7	0.59
5	m16-000	160.0	0.0	0.00	1.6	100.0	-	179	320	24.2	25.7	1.00
6	m16-375	160.0	37.5	0.23	1.6	100.0	23.4	179	320	24.2	25.7	0.98
7	m16-750	160.0	75.0	0.47	1.6	100.0	46.9	179	320	24.2	25.7	0.86
8	m16-1125	160.0	112.5	0.70	1.6	100.0	70.3	179	320	24.2	25.7	0.64
9	m23-000	160.0	0.0	0.00	2.3	69.6	-	179	320	24.2	25.7	1.00
10	m23-375	160.0	37.5	0.23	2.3	69.6	16.3	179	320	24.2	25.7	0.99
11	m23-750	160.0	75.0	0.47	2.3	69.6	32.6	179	320	24.2	25.7	0.89
12	m23-1125	160.0	112.5	0.70	2.3	69.6	48.9	179	320	24.2	25.7	0.68

D_o, D_i : outer and inner tube's diameters, t_i, t_o : inner and outer tube's thicknesses, E_s, E_c : young's modulus of steel tubes and filled concrete, f_y : yielding point of steel tubes, f_c : concrete cylinder strength, M_u : bending strength calculated using Eqs. (2) and (2)'.

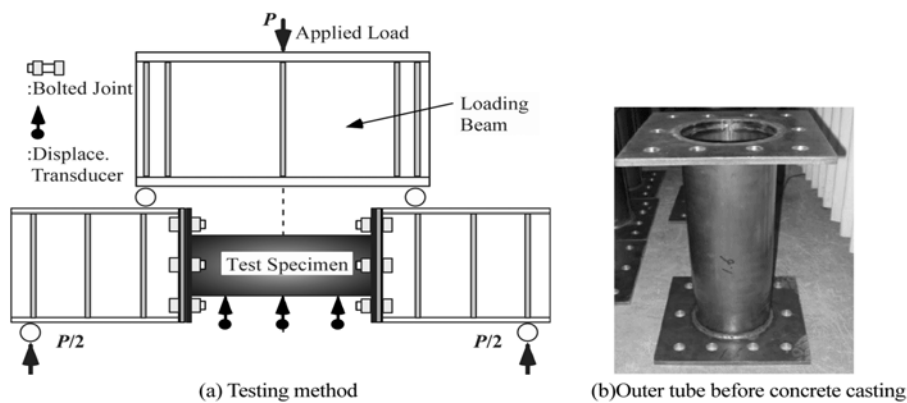


Fig. 2 Test apparatus

connected to a strong side beam with high tension bolts, as shown in Fig. 2(b). While, the inner tube could not welded to the end plate. Because a narrow space between both the tubes could not make biaxial strain gauges attach on the inner tube after the welding. Moreover, the gauges go wrong owing to welding heat when they attach before welding. Influence of no welding joint of the inner tube to the end plates will be discussed later. The symmetric four points loading test apparatus used herein is illustrated in Fig. 2. A pure bending action was applied to all the specimens by using the apparatus.

2.2 Estimated bending strength

Longitudinal stress distributions due to bending action of the inner and outer tubes and the filled concrete

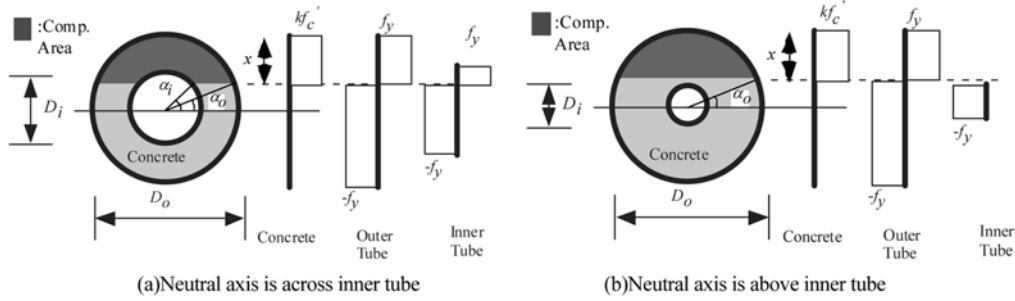


Fig. 3 Cross section and ultimate stress distribution of CFDST

at ultimate state can be assumed as shown in Fig. 3, based upon Bernoulli assumption in collaboration with an equivalent stress block method. As shown in Fig. 3(a), when a neutral axis is across the inner tube area, ultimate bending moment : M_u and axial force : N_u are expressed as:

$$M_u = \frac{2kf'_c}{3}(R_o^3 \cos^3 \alpha_o - R_o^3 \cos^3 \alpha_i) + 4f_y(R_o^2 t_o \cos \alpha_o + R_i^2 t_i \cos \alpha_i) \quad (1)$$

$$N_u = \frac{\pi kf'_c}{2} \left\{ R_o^2 \left(1 - \frac{2\alpha_o}{\pi} - \frac{\sin 2\alpha_o}{\pi} \right) - R_i^2 \left(1 - \frac{2\alpha_i}{\pi} - \frac{\sin 2\alpha_i}{\pi} \right) \right\} - 4f_y(R_o t_o \alpha_o + R_i t_i \alpha_i) \quad (2)$$

where, f_y : yielding point of the steel tubes; f'_c : cylinder strength of compressive concrete; k : equivalent stress block coefficient of 0.85; R_i and R_o : radii of the inner and outer tubes; t_i and t_o : the inner and outer tube thickness and α_i and α_o : angles between the horizontal centroid axis and radial lines across the neutral axis at the inner and outer tubes diameters, respectively. Otherwise, if a neutral axis exists above the inner tube as shown in Fig. 3(b), the estimation equations relevant to Eqs. (1) and (2) should be modified as follows:

$$M_u = \frac{2kf'_c}{3} R_o^3 \cos^3 \alpha_o + 4f_y R_o^2 t_o \cos \alpha_o \quad (1)'$$

$$N_u = \frac{\pi kf'_c}{2} R_o^2 \left(1 - \frac{2\alpha_o}{\pi} - \frac{\sin 2\alpha_o}{\pi} \right) - 4f_y t_o \left(\alpha_o R_o + \frac{R_i}{2} \pi \right) \quad (2)'$$

Ultimate strength under pure bending action also can be estimated as follow steps: First, a tentative solution satisfied with no axial action condition in Eq.(2) or Eq(2)' is sought by an iteration method with a prescribed incremental angle of α ; Second, the convergent angle of α is introduced into Eq.(1) or Eq.(1)' to obtain the estimated ultimate strength: M_u . It is noted additionally that a well known design formula for CFT members (the Architectural Institute of Japan (1997)) recommends that compressive and tensile strengths of the steel tube should be $\beta_1 f_y$ where β_1 is 0.89 and $\beta_2 f_y$ where β_2 is 1.08, respectively. However, these correction coefficients are identical each other to be unit herein.

Fig. 4 (a),(b) and (c) show the cross sections of the existing CFDST bending test specimens. Next,

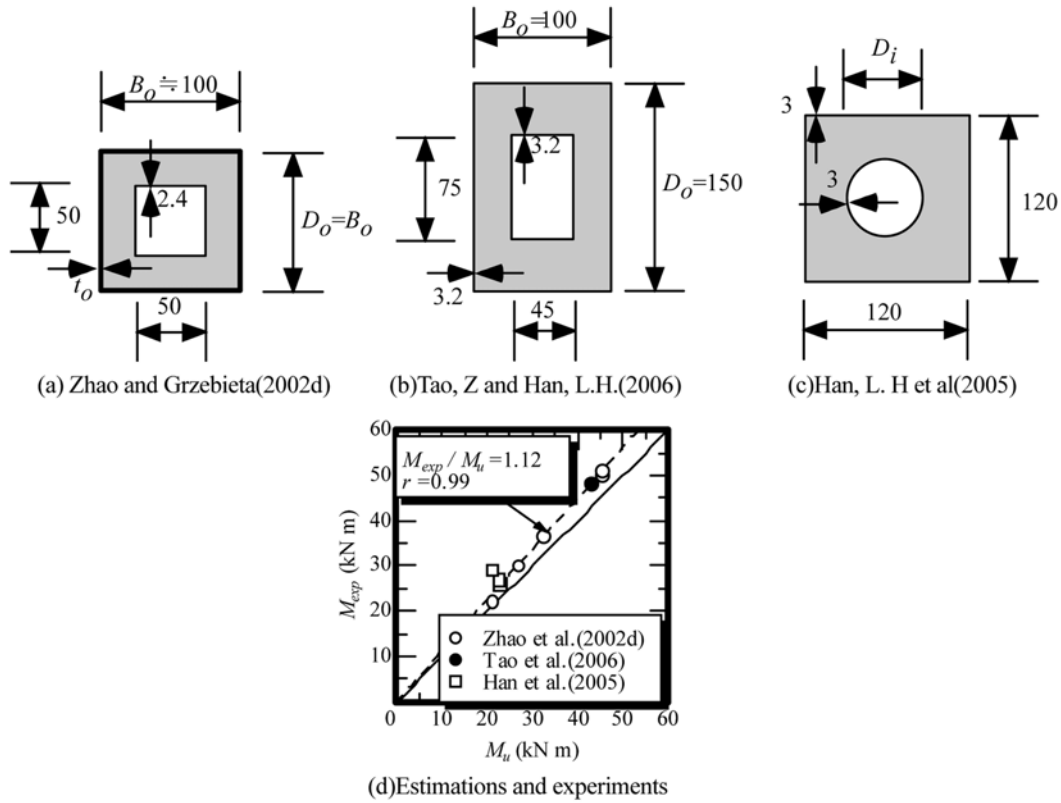


Fig. 4 Verification of proposed bending strength estimation based on existing experimental strength (unit: mm)

Fig. 4(d) shows the relation between the estimated strengths by Eq(1) under $N_u = 0$ and experimental ultimate strengths M_{exp} . It could be found a fair agreement between them.

2.3 Measurements

As shown in Fig. 5, a total of twenty four biaxial strain gauges were attached to the outsides of the

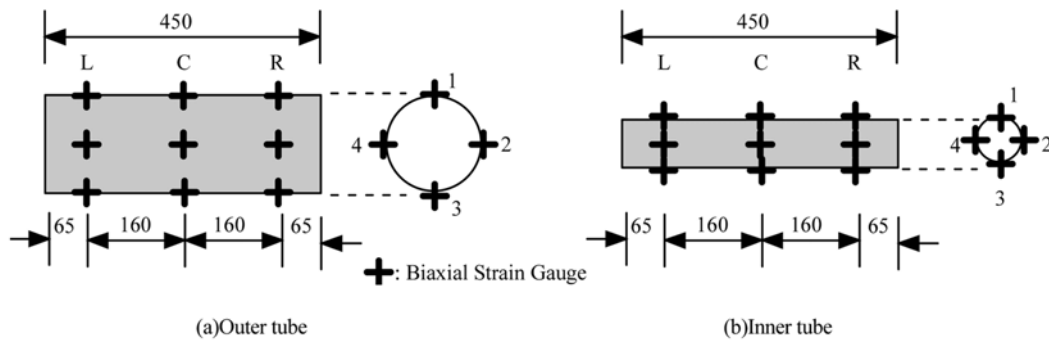


Fig. 5 Positions of strain gauge

inner and outer tubes to observe their stress distributions. Furthermore, three displacement transducers to measure vertical displacements, so-called deflection, were arranged at the span central position as shown in Fig. 3 with 160 mm interval.

3. Results and Discussions

3.1 Failure Mode

The observed failure modes of the outer tubes were controlled by local buckling and tensile cracking as shown in Figs.6(a) and (b). Excepting the specimen of “m-10-1000” in which the outer tube was folded to break at its mid span, all of the rest specimens were failed near their end joint plates. Moreover, no local buckling of the inner tubes could be found though their tensile yielding could be confirmed.

For the specimens with large inner tubes' diameters, a local bending moment near the end plates occurred probably because of the filled concrete contribution to prevent the inner tubes from their out-plane buckling. Consequently, progressive breaking behavior around the bolt joint portion, thus, could be observed in an early loading stage(see Figs. 5(c) and (d)).

Fig. 7 shows axial strain distribution of inner and outer tubes with the largest D_i/D_o . In the figure, almost linear strain distribution can be seen at the span center section on the whole loading stage, but the strain distribution at the end sections much deviates from a linear distribution on the higher loading stage. Such a phenomenon suggests slip occurrence on the end portions of inner tube because of no connection between the inner tube and the end plates. However, it should be noted that the load carrying capacities obtained in the tests exceed the estimated values under Bernoulli assumption, as shown in Fig. 7. Further effect of no welding joint between the inner tube and the end plates on the test

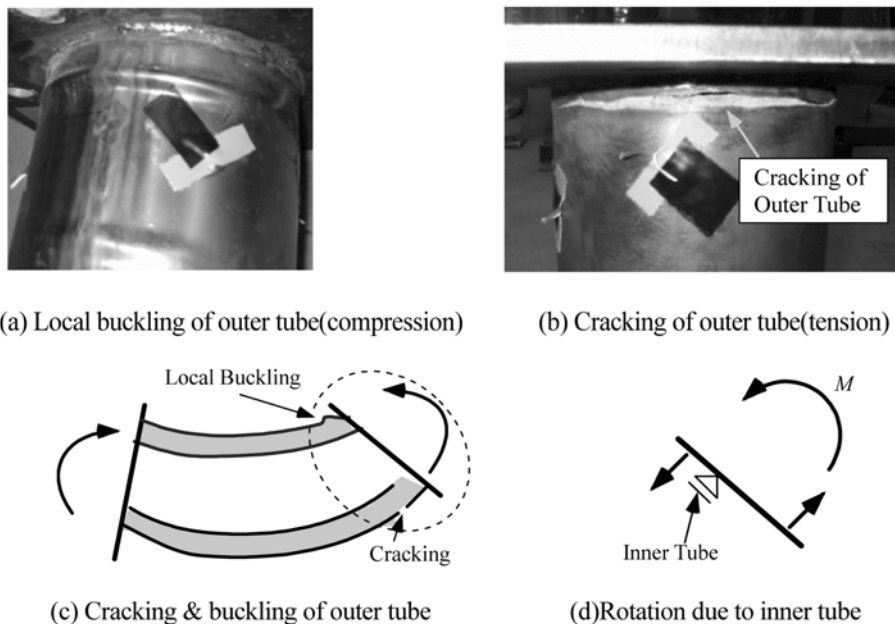


Fig. 6 Failure mechanism

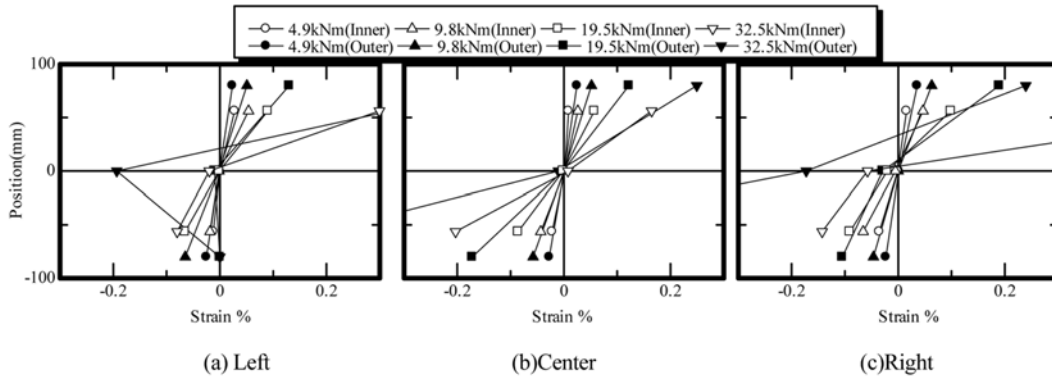


Fig .7 Strain distribution(m23-1125)

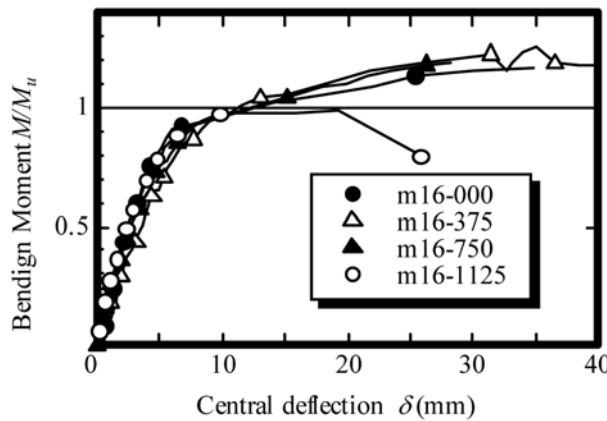


Fig. 8 Central Deflection and Normalized Moment

results remains as a future problem to be solved in order to refine the load-deflection curves of Fig. 8.

3.2 Bending Strength

Fig. 9 and Table 2 show the relationship between the measured bending strengths given by $P_{max} a / 2$, where P_{max} and a are maximum applied load and shear span length, respectively, and the relevant estimated values by Eq.(1) or Eq.(1)' when N_u are equal to zero. The measured strengths were almost same as or somewhat larger than the estimated values, in which the statistical correlation factor: r was 0.95 and the average ratio of the measured strength to the estimate values: M_{exp} / M_{u0} was 1.13. Furthermore, the measured strengths of CFT specimens arose by 23%~47% from the relevant estimated values. Whereas, the ratio: M_{exp} / M_{u0} decreased as the inner-to-outer tubes' diameter ratio: D_i / D_o increased as shown in Fig. 9(a). It could be suggested, thus, that the strength enhancement due to the confinement effect on the filled concrete was the most remarkable for the CFT specimens and also that the enhancement for CFDT specimens gradually decreased as D_i / D_o increased.

Furthermore, the estimation could be improved as shown in Fig. 10b if the ultimate moment was

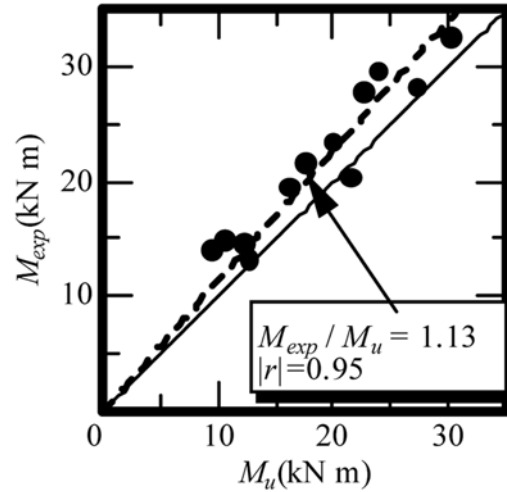


Fig. 9 Estimated and experimental strength

Table 2 Test Results

No.	Tag	D_i / D_o	M_u (kN m)	M_{exp} (kN m)	M_{exp} / M_u
1	m10-000	0.00	9.5	14.0	1.47
2	m10-375	0.23	10.6	14.8	1.39
3	m10-750	0.47	12.3	14.6	1.19
4	m10-1125	0.70	12.7	13.1	1.03
5	m16-000	0.00	16.2	19.5	1.20
6	m16-375	0.23	17.6	21.6	1.23
7	m16-750	0.47	20.0	23.4	1.17
8	m16-1125	0.70	21.5	20.3	0.94
9	m23-000	0.00	22.6	27.7	1.23
10	m23-375	0.23	23.9	29.6	1.24
11	m23-750	0.47	27.3	28.2	1.03
12	m23-1125	0.70	30.2	32.5	1.07

calculated again introducing ultimate tensile strength $f_u = 400$ MPa instead of relevant yielding point f_y . It could be suggested that significant strain hardening was occurred when $D_i /$ is less than 0.25. The test results were agree with the re-estimations rather than bending strength based on yielding point, which suggested the strength enhancement due to strain hardening of the steel tubes, in particular, for the specimens with smaller D_i / D_o .

3.3 Normalized moment and curvature

Fig. 11 shows the relationship between the normalized bending moment: M / M_u and curvature: ϕ , in which the latter was obtained based on the measured deflections at three points with the equivalent

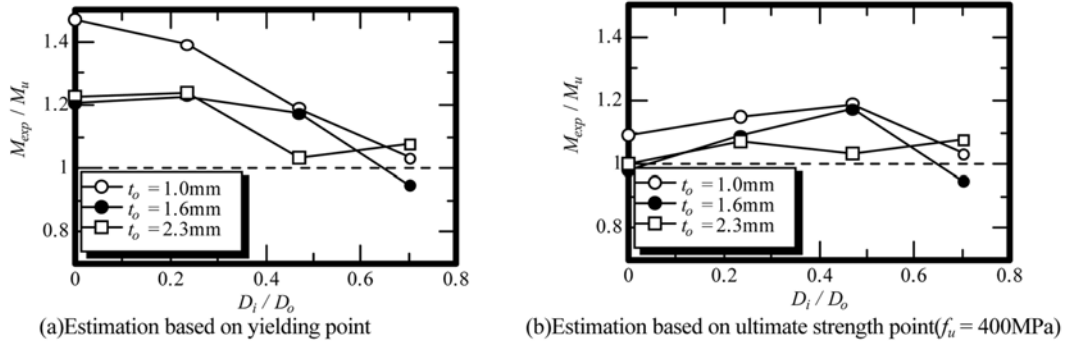


Fig. 10 D_i / D_o and normalized moment

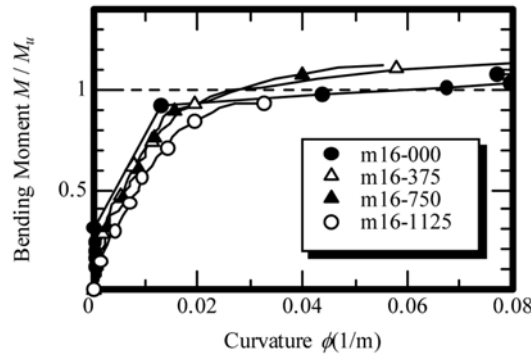


Fig. 11 Curvature and Normalized Moment

interval by means of a finite difference method. All the specimens, except for the specimen of “m16-1125”, showed similar behaviors in an early stage within ϕ less than 0.02(1/m). After cracking in the filled concrete, however, the rigidity decreased gradually. Further discussion on the confined effect will be given later.

3.4 Calculation of elasto-plastic stresses

3.4.1 Characteristics of elasto-plastic stresses

A thin steel tube in pure bending state may be subjected to biaxial stresses, σ_z and σ_θ in axial and circumferential directions, respectively. Assuming perfectly plastic material subjected to von Mises yield criterion, the corresponding yield condition for a plane stress problem is expressed as

$$f_s = \sigma_z^2 - \sigma_z \sigma_\theta + \sigma_\theta^2 - f_y^2 = 0 \tag{3}$$

where f_{sy} is yield point of steel tube. As indicated in Figs 12 and 13, when the circumferential stress, σ_θ , is tension, a compressive confinement stress (σ_{3o}) from the outer tube is induced to in-filled concrete. On the other hand, when σ_θ is compression, the corresponding confined stress (σ_{3i}) from the inner tube is also induced to in-filled concrete. Namely,

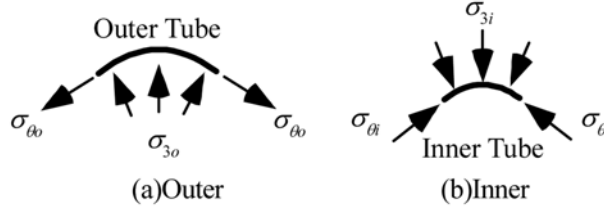


Fig. 12 Stress conditions of double tubes



Fig. 13 Stress conditions of filled concrete

$$\sigma_{3o} = \frac{2t_o \sigma_{\theta o}}{D_o} \quad \text{and} \quad \sigma_{3i} = \frac{2t_i \sigma_{\theta i}}{D_i} \quad (4), (5)$$

where D_i and D_o are inner and outer diameters, respectively.

When the tubes remain in an elastic range, namely $f_s < 0$, relationship between stress rate, $d\sigma = [d\sigma_z \ d\sigma_\theta]^T$, and strain rate, $d\varepsilon = [d\varepsilon_z \ d\varepsilon_\theta]^T$, are follows:

$$d\sigma = \mathbf{C}_{se} d\varepsilon \quad (6)$$

where \mathbf{C}_{se} is elastic stress-strain matrix, namely,

$$\mathbf{C}_{se} = \frac{E_s}{1-\nu^2} \begin{bmatrix} 1 & \nu \\ \nu & 1 \end{bmatrix} \quad (7)$$

On the other hand, when the tubes enter an elastic-plastic zone, namely $f_s = 0$, elastic strain increment $d\varepsilon^e$, and plastic strain increment, $d\varepsilon^p$, are combined, and $d\varepsilon^p$ is according to the associated plastic flow rule as

$$d\varepsilon^p = d\lambda \left[\frac{\partial f_s}{\partial \sigma} \right] \quad (8)$$

where $d\lambda$ plastic flow coefficient which is a positive scalar factor. Using consistency condition, being

$$df_s = \frac{\partial f_s}{\partial \sigma_z} d\sigma_z + \frac{\partial f_s}{\partial \sigma_\theta} d\sigma_\theta = 0 \quad (9)$$

a and Eq.(6), one obtain

$$d\lambda = \frac{\left[\frac{\partial f_s}{\partial \sigma} \right]^T \mathbf{C}_{se} d\boldsymbol{\varepsilon}}{\left[\frac{\partial f_s}{\partial \sigma} \right]^T \mathbf{C}_{se} \left[\frac{\partial f_s}{\partial \sigma} \right]} \quad (10)$$

where $d\lambda$ is effective when $d\lambda > 0$, and the following elastic-plastic constitutive relation can be obtained

$$d\boldsymbol{\varepsilon} = \mathbf{C}_{sep} d\boldsymbol{\varepsilon} \quad (11)$$

where,

$$\mathbf{C}_{sep} = \mathbf{C}_{se} \left\{ \bar{\mathbf{E}} - \frac{\left[\frac{\partial f_s}{\partial \sigma} \right] \left[\frac{\partial f_s}{\partial \sigma} \right]^T \mathbf{C}_{se}}{\left[\frac{\partial f_s}{\partial \sigma} \right]^T \mathbf{C}_{se} \left[\frac{\partial f_s}{\partial \sigma} \right]} \right\}, \text{ then, } \boldsymbol{\sigma} = [\sigma_z \ \sigma_\theta]^T, \left[\frac{\partial f_s}{\partial \sigma} \right] = [2\sigma_z - \sigma_\theta \ 2\sigma_\theta - \sigma_z]^T, \bar{\mathbf{E}} = \begin{bmatrix} 1 & 0 \\ 0 & 1 \end{bmatrix}$$

The biaxial strain gauges attached on both the outer and inner tubes follow strain trajectories and then the corresponding stress histories can be found from Eq.(11), in which strain rate is replaced by small incremental measurement of strain. Namely,

$$\begin{bmatrix} \Delta\sigma_{zn} \\ \Delta\sigma_{\theta n} \end{bmatrix} = \mathbf{C}_{se} \begin{bmatrix} \Delta\varepsilon_{zn} \\ \Delta\varepsilon_{\theta n} \end{bmatrix}, \text{ or, } \begin{bmatrix} \Delta\sigma_{zn} \\ \Delta\sigma_{\theta n} \end{bmatrix} = \mathbf{C}_{spe} \begin{bmatrix} \Delta\varepsilon_{zn} \\ \Delta\varepsilon_{\theta n} \end{bmatrix} \quad (12a,b)$$

Therefore, the whole stress histories in the test specimens can be obtained from

$$\begin{bmatrix} \sigma_z \\ \sigma_\theta \end{bmatrix} = \sum_n \begin{bmatrix} \Delta\sigma_{zn} \\ \Delta\sigma_{\theta n} \end{bmatrix} \quad (13)$$

In practice, measured strain increments being 1/10 of yield strain were used and elasto-plastic stress and strain response could be found by Eqs.(12) and (13), until local buckling or tensile fracture occurred.

3.4.2 Stress histories under compression due to bending

As a representation of stress histories of the tubes, their elasto-plastic stress paths on a biaxial stress plane could be drawn by Eqs. (12) and (13) based upon the measured strains by the biaxial strain gauges attached both inner and outer tubes as shown in Fig. 5. Figs. 14 and 15 show the stress paths of the outer and inner tubes, respectively, in which the view point is located on the top of each tube at mid

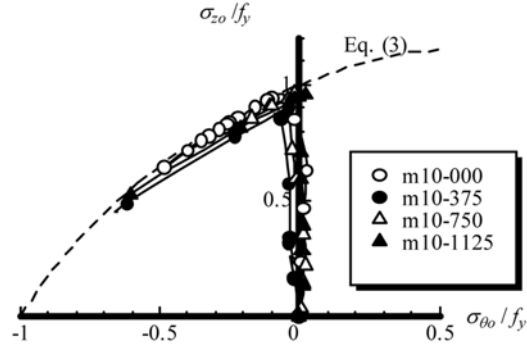


Fig. 14 Stress histories of outer tube(bending-compression)

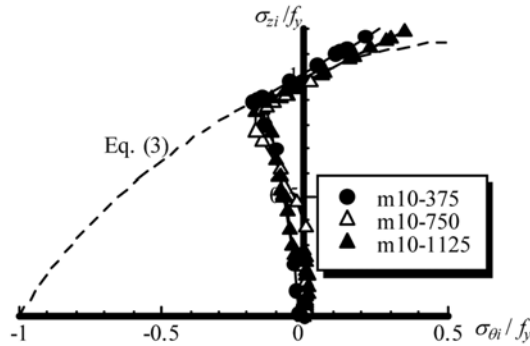


Fig. 15 Stress histories of inner tube(bending-compression)

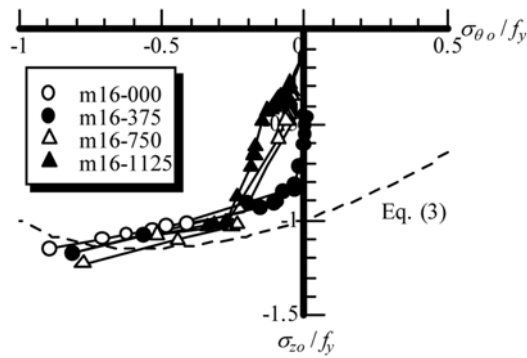


Fig. 16 Stress histories of outer tube(bending-tension)

span as shown Figs. 2 and 5. The coordinates of these figures are normalized by the yielding point of the tube: f_y . Moreover, positive value indicates normalized compressive stress intensity, and also the broken curves denote the von Mises yield condition of Eq. (3). As shown in Fig. 14, after yielding, the stress paths of the outer tubes flowed toward a tensile zone along the yield condition curve. Consequently, a confined stresses arose due to volumetric dilatation of the filled concrete. Whereas, the paths of the

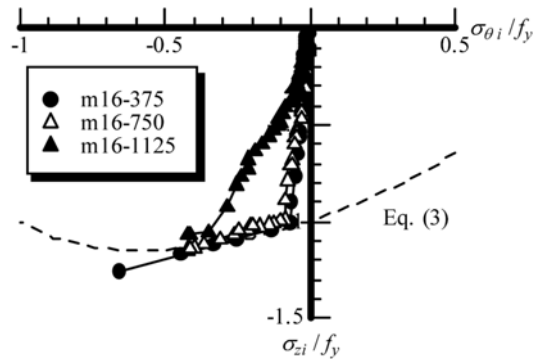


Fig. 17 Stress histories of inner tube(bending-tension)

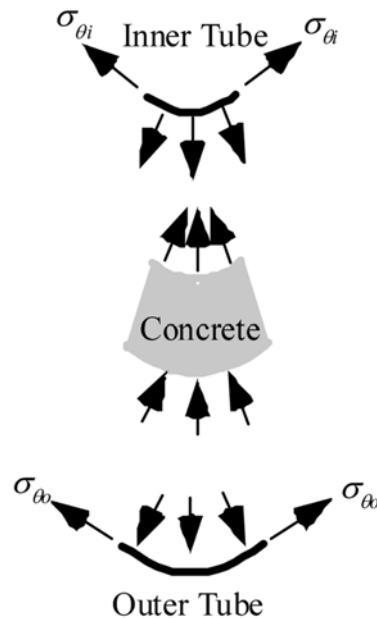


Fig. 18 Stress Conditions of Tensile Region

inner tubes flowed toward a compressive zone to give the filled concrete a confinement action as shown in Fig. 15. Thus, it could be recognized that CFDT members develop a significant confined effect in compressive region due to bending.

3.4.3 Stress histories under tension due to bending

Figs. 16 and 17 show the stress histories in a bending-tensile region of both the outer and inner tubes which were derived from the bottom gauges at the span center. The axial stress, σ_{zo} , appears in the tensile range under the effect of bending, but the circumferential stress, $\sigma_{\theta o}$, also flows to the tensile side. Such phenomena may suggest an existence of confinement stress in the in-filled concrete based on a stress transmission mechanism as shown in Fig. 18.

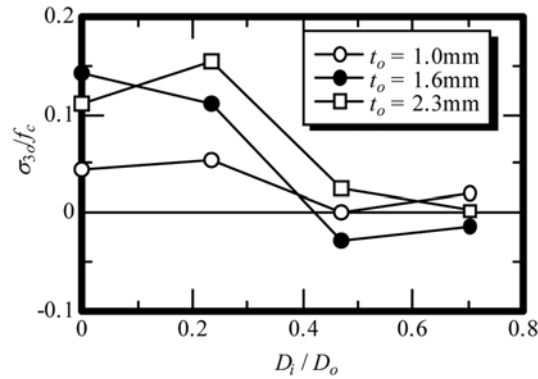


Fig. 19 Maximum confined stress(outer tube)

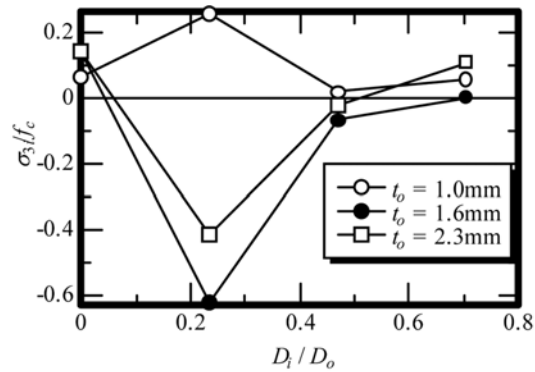


Fig. 20 Maximum confined stress(inner tube)

3.4.4 Intensity of Confinement Stress

Figs. 19 and 20 shows the relationships between the confinement stresses induced into the filled concrete and the inner-to- outer diameter ratio, assuming the circumferential compressive stresses in the both tubes can meaningfully related to the confinement stresses. In the outer tubes, a significant confinement stresses appeared when the ratio: D_i/D_o was less than 0.45, where the maximum stress intensity attained to 0.15 times as large as the cylinder strength of compressive concrete: f_c' . However, in the inner tubes, the confinement stresses were not noticeable because of the effect of large tensile stress due to bending caused an upward shift of the neutral axis in elasto-plastic region

4. Conclusions

Mechanical behavior of the concrete filled double steel tubular: CFDST members subjected to bending is investigated experimentally in comparison with the ordinary concrete filled steel tubular: CFT member. The following remarks can be drawn:

- The observed CFDST failure modes were local buckling in compression and cracking in tension of the outer steel tube. The cracking occurred near the end joint plate due to local bending of the inner

tube in early loading stage.

- Bernoulli assumption was sufficiently satisfied from the view point of the axial strain distributions. However, scattering of strain distributions were observed near the ultimate moment M_u because of concrete cracking.
- The measured CFDST bending strengths were almost same as or slightly larger than the relevant well known estimated values. The strengths gradually decreased as the inner-to-outer tube diameter ratio increased. Furthermore, the estimation was improved if the ultimate moment was calculated again introducing ultimate tensile strength $f_u = 400$ MPa.
- Flexural rigidities of CFDST with 16 mm in tube thickness were almost same as those of the ordinary CFT, except for the specimen of “m16-1125” with the largest ratio of the inner-to-outer tube diameter. Plastic deformability of CFDST up the curvature of 0.04(1/m) was also same as that of CFT, excepting CFDST with the largest ratio of the inner-to-outer diameter showed an inferior behavior.
- The observed outer tubes' stress paths under compression due to bending flowed toward tensile zone after yielding. On contrary, the corresponding inner tubes' paths flowed toward compressive zone. It could be suggested an essential existence of the confinement stress on the filled concrete.
- The confinement stresses on the filled concrete under compression due to bending existed in case of the inner-to-outer tube diameter less than 0.45, where the maximum intensity attained to 0.15 times as large as the cylinder strength of compressive concrete.
- The confinement stresses under the tension due to bending, however, were not confirmed clearly because of the effect of large bending tensile stress leading the upward neutral axis shift.

Acknowledgement

We would like to thank Mrs. Y. Nishida, M. Gotoh, K. Hashimoto and R. Gotoh for their sincere helps to this study. It should be also noted that a part of the study was financially supported by Grant-in-Aid for Science Research, Japan Society for the Promotion of Science.

References

- Architectural Institute of Japan (2002), *Standard for Structural Calculation of Steel Reinforced Concrete Structures*. (in Japanese)
- Wei, S., Mau, S.T., Vipulanandan, C. and Mantrala, S.K. (1995a) “Performance of New Sandwich Tube under Axial Loading: Experiment”, *Jour. of Struct. Eng.*, American Society of Civil Eng., **121**(12), pp. 1806-1814.
- Wei, S., Mau, S.T., Vipulanandan, C. and Mantrala, S.K. (1995b) “Performance of New Sandwich Tube under Axial Loading: Analysis”, *Jour. of Struct. Eng.*, American Society of Civil Eng., **121**(12), 1815-1821.
- Zhao, X. L., Grzebieta, R.H. and Elchalakani, M. (2002a) “Tests of Concrete-filled double skin CHS composite stub columns”, *Steel and Composite Structures – An International Journal*, **2**(2), 129-142.
- Zhao, X. L., Grzebieta, R. H., Ukur, A. and Elchalakani, M. (2002b) “Tests of concrete-filled double skin (SHS Outer and CHS inner) composite stub columns”, *Advances in Steel Structures*, **1**, Chan, Teng and Chung (Eds.), Elsevier, 567-574.
- Elchalakani, M., Zhao, X. L., and Grzebieta, R.(2002c) “Tests on concrete filled double-skin(CHS outer and SHS inner) composite short columns under axial compression”, *Thin-Walled Structures*, **40**(5), 415-441.
- Zhao, X. L, and Grzebieta, R. (2002d) “Strength and ductility of concrete filled double skin (SHS inner and SHS outer) tubes”, *Thin-Walled Structures*, **40**(5), 199-213.

- Zhao, X.L. and Han, L.H. (2006), Double Skin Composite Construction, *Progress in Structural Engineering and Materials*, **8**(3), 93-102.
- Tawaratani, Y. and Kurita, A. (1999) "Stress-Strain Relationship for Concrete in Concrete-Filled Double Steel Tubular Columns", *Proc. of 5th Korea-Japan Joint Seminar on Steel Bridges*, Pusan, Korea, 151-162.
- Yagishita, F., Kitoh, H., Sugimoto, M, Tanihira, T. and Sonoda, K. (2000) "Double Skin Composite Tubular Columns subjected to Cyclic Horizontal and Constant Axial Forces", *Composite and Hybrid Structures*, University of Southern California, U.S.A. , **1**, 497-503.
- Uenaka, K., Kitoh, H. Sonoda, K. and Hayami, M. (2003), "Experimental Study on Concrete Filled Double Tubular Steel Columns under Axial Loading", *Advances in Structures*, A.A.Balkema Publishers, Netherlands, **2**, 877-882.
- Han, L. H., Tao, Z., Huang, H. and Zhao, X. L.(2004), "Concrete-filled double skin(SHS outer and CHS inner) steel tubular beam-columns", *Thin-Walled Structures*, **42**(9), 1329-1355.
- Tao, Z. and Han, L.H.(2005), "Behavior of Concrete-filled Double Skin Rectangular Steel Tubular beam-columns", *J. Constr. Steel. Res.*, **62**(7), 631-646.